Volume 3 Issue 2 (September 2023)
DOI 10.24191/jaeds.v3i2.67
eISSN 2805-5756

Journal of Applied Engineering Design & Simulation

Residual Stress Measurements on SS316L Specimen using Selective Laser Melting and Numerical Computation Software

Micheal Stoschka[1], Liyana Balqis[2,3,*], Stefan Fladischer[1], Thoufeili Taufek[2,3], Yupiter HP Manurung[2,3], Mohd Shahriman Adenan[2,3] and Renga Rao Krishnamoorthy[2,3]
[1]Chair of General Mechanical Engineering, Montanuniversität Leoben, 8700, Austria.
[2]Smart Manufacturing Research Institute, Universiti Teknologi MARA, Shah Alam 40450 Selangor, Malaysia.
[3]School of Mechanical Engineering, Universiti Teknologi MARA, Shah Alam 40450 Selangor, Malaysia.
[*]Corresponding author: 2020334311@student.uitm.edu.my

ABSTRACT

This research aimed to predict the residual stress of additively manufactured rectangular specimen using Selective Laser Melting (SLM) by means of non-linear numerical computation based on Thermo-mechanical method (TMM). The procedure started with the geometrical and material modelling of rectangular specimen with regard to Austenitic Stainless Steel 316L (SS316L) in which the temperature dependent material data properties such as Young's Modulus, Thermal Expansion Coefficient, Specific Heat Capacity and Thermal Conductivity were considered. The next phase consisted of numerical computation procedure in which the specimen was positioned 60° of inclination angle from the substrate plate. The support structure was to be generated within the lower surface of the specimen in order to avoid the material from collapsing during printing process. Laser heat source was modelled based on the laser beam width, power, efficiency and scanning speed in order for the numerical computation to accurately predict the thermal problem of SLM process. Furthermore, layer parameters used to fabricate the specimen such as hatch distance, hatch scan width and layer thickness were taken into TMM consideration. Similar set-up from numerical computation by means of laser and layer parameters to fabricate SS316L rectangular specimen was utilized in real fabrication process using SLM machine, Renishaw RenAM 500E. After fabrication of the specimen, electropolishing as for the sample preparation of X-Ray Diffraction (XRD) measurement was conducted by means of various depths on both sides of the specimen. For the validation procedure, residual stress on every depth was analysed and compared with the result from numerical computation. In conclusion, TMM simulation forecasted an acceptable residual stress of SLM product with relative error up to 14% and the computational time taken to predict the residual stress was only 56 minutes. This exploratory research using TMM simulation to predict residual stress of SLM product could benefit metal additive manufacturing (MAM) production as a whole by neglecting expensive trial and error approach.

Keywords: Residual stress; Simufact Additive 2022; Selective Laser Melting (SLM); X-Ray Diffraction (XRD); SS316L; Thermo-mechanical method (TMM); Metal Additive Manufacturing (MAM).

Abbreviations

CAD	Computer-Aided Design
SLM	Selective Laser Melting
MAM	Metal Additive Manufacturing
AM	Additive Manufacturing
TMM	Thermo-mechanical method
XRD	Xray-diffraction

1.0 INTRODUCTION

Additive Manufacturing (AM), widely known as 3D Printing, is a manufacturing method which produces three-dimensional products by layering materials by layer. It is in contrast to subtractive manufacturing technique, which removes material to form the final result. Charles Hull produced the process of stereolithography (SLA) in 1986, which was then followed by innovations like powder bed fusion, fused deposition modelling (FDM), inkjet printing and contour crafting (CC) [1]. Over the past three decades, advancements in materials and methods, coupled with ingenious design, have led to successful commercialization [2]. This approach reduces time, cost, human interaction, the product development cycle and it allows the creation of any shape that would be difficult to machine [3]. The scale of the parts that can be fabricated with AM ranges from small to large, but the precision

Received on 25.08.2023
Accepted on 01.10.2023
Published on 10.10.2023

of the printed piece is determined by the process that is used along with the scale at which the printing is done. The sequence begins with a digital model of the object that is developed using computer-aided design (CAD) software. Aerospace, automotive, medical and consumer products are a few of the industries that utilize AM. It has also been applied in architecture and arts. For instance, the application of AM to create functioning goods with anticipated mechanical structural qualities has increased in recent years and it allows doctors to analyse a patient's wounds and market researchers to understand what consumers think of a new product more accurately [4]. There are several types of additive manufacturing processes including VAT Photopolymerization, Material Jetting, Binder Jetting, Material Extrusion, Powder Bed Fusion, Sheet Lamination and Directed Energy Deposition [5]. Powder Bed Fusion uses a laser or electron beam to selectively melt or fuse powdered materials which usually consist of plastic or metal and come in a variety of forms including SLM.

In additive manufacturing of metals, a powder feedstock is entirely melted by the energy input of a laser or electron beam, and it changes layer by layer into any solid part geometry [6]. There are many different types of MAM technologies, which may be categorised according to the energy source, the type of feeding material, the technique in which the feeding material is provided and the way in which the layers are joined (based on fusion or non-fusion) [7]. When compared to more traditional methods, the thermodynamics and solidification rates of MAM are different because it is a non-equilibrium process involving rapid melting and cooling cycles.

Before CAD data can be sent to the SLM machine for component production, the STreoLithography (STL) files must be analysed by software to build support structures for any overhanging elements and slice information for laser scanning of different layers. In the SLM process, laser energy is used to melt metallic powders without agents one at a time, forming solid models in the subsequent layers. The powder bed is where the laser beam is focused after traveling through the optical fibre. The models are constructed on a base plate within the chamber containing nitrogen gas [8]. Literature demonstrates that SLM is capable of completely melting the powder material which leads in very dense near-net-shape components that require no post-processing beyond the removal of pieces and support from the substrate plate. As a result of the high heating and cooling rates involved with cycling, the interaction between the laser and the powder generates large temperature gradients in the part during the manufacturing process [9]. These heat effects produce significant residual stresses and plastic strains.

In post-processing by machining and heat treatment, residual stress results in cracks and deformation of the specimen while fatigue strength of the specimen is decreased when tensile stress persists close to the specimen surface. Residual stress is the stress remaining in a material after the removal of external pressures. It can damage the performance and dependability of the material, and it also leads to its failure under certain conditions. Many researchers have addressed the several damaging post-process techniques used to detect residual stress. During the heating state, a heat source that has a high energy intensity quickly heats up the feed stock material, and the heated material tends to expand. However, this thermal expansion is restrained by the surrounding materials, which have a lower temperature. The previously formed heated zone starts to cool down when the heat source is removed, and materials in this zone tend to shrink as a result. Nevertheless, the shrinkage of these materials is partially limited by the plastic strain that is formed during the heating step [10]. Considering MAM is characterized by its layer-by-layer construction process, the cool-down phase model provides an additional explanation for the mechanism of residual stress production in MAM [11,12].

Non-destructive testing technology is a vital and effective method which has gained widespread acceptance and become the future standard for measuring residual stresses. Methods include measuring mechanical distortion, X-ray and neutron diffraction, light scattering changes in elastic wave speeds and magnetic field changes owing to stress relaxation or rise [13]. X-Ray Diffraction analysis is a method of non-destructive testing which is utilized for the purpose of measuring the amount of residual stress present in a material. Diffraction is a phenomenon involving the scattering of X-rays by the atoms of a crystal and the strengthening of scattered rays in specific directions away from the crystal [14]. Analysing the pattern X-Ray Diffraction reveals information on the arrangement of atoms in a material including their positions and distances from one another. Since the measurement is assumed to be near the surface, X-rays may penetrate some length into the material; thus, the penetration depth depends on the material, the angle of incidence and the anode.

The precise measurement and analysis of residual stresses are necessary to preserve the integrity and reliability of SLM-manufactured outcomes. This research aims to analyse the residual stress distribution in detail by determining stress magnitude using numerical computation software and post-processing procedures. In this study, residual stress was investigated utilizing Thermo-mechanical approach by numerical non-linear computation.

2.0 EXPERIMENT SETUP AND PROCEDURES USING SLM

The methodology centred on analysing residual stresses of rectangular specimen SS316L by performing simulation and experiment method of this research. To ensure that the project would proceed in the direction of the outcome that was initially anticipated, the goals and objectives of the project were defined after gaining a thorough understanding of it as well. Figure 1 is a flowchart depicting how this project is implemented.

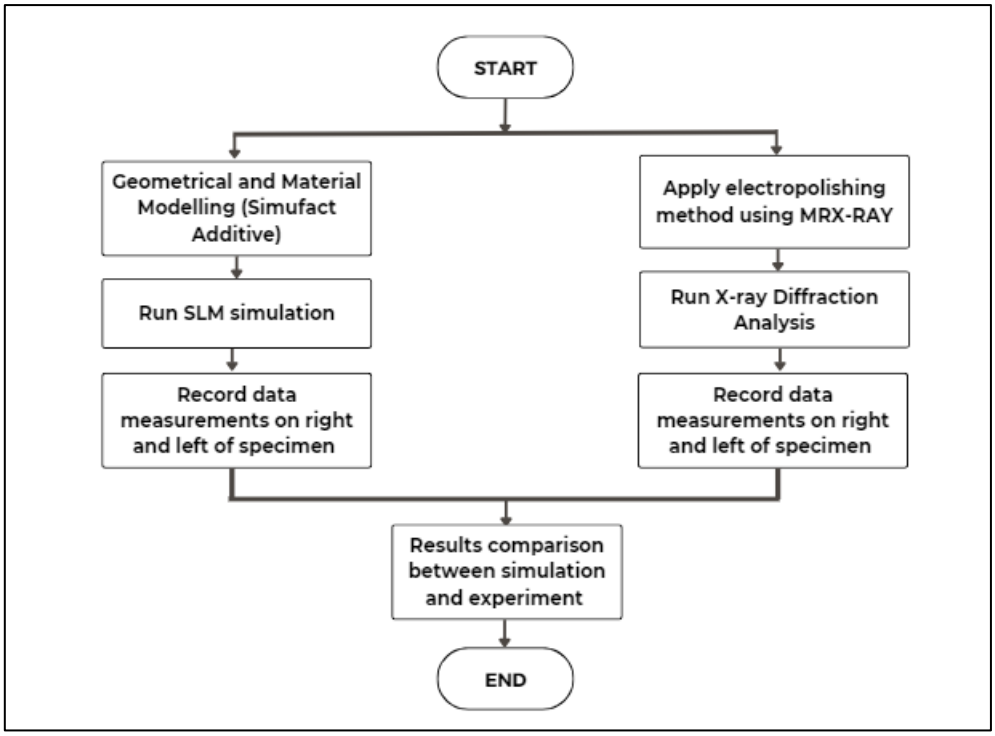

Figure 1. The flowchart of project methodology

To begin, a rectangular specimen made of Austenitic Stainless Steel 316L (SS316L) is modelled geometrically and materially with consideration given to temperature-dependent material data properties like Young's Modulus, Thermal Expansion Coefficient, Specific Heat Capacity and Thermal Conductivity. SLM is performed on Renishaw RenAM 500E with confined atmosphere. A support structure must be generated on the specimen's base to prevent material from collapsing during the printing process. In order for the numerical computation to accurately forecast the thermal problem in the SLM process, the laser heat source must be modelled based on laser beam width, power, efficiency, and scanning speed. In addition, TMM considers the layer characteristics utilised to produce the specimen such as hatch distance, hatch style (Bi-directional), hatch scan width and layer thickness. Table 1 shows the parameters of the manufacturing process.

Table 1: Experimental parameters using Renishaw RenAM 500E for SS316L

Process Parameters	Dimension
Laser beam power (W)	195
Laser scanning speed (mm/s)	750
Hatch distance (mm)	0.11
Layer thickness (mm)	0.05

3.0 SIMULATION ANALYSIS ON RESIDUAL STRESS

3.1 Geometrical modelling

Simufact Additive 2022 is a comprehensive software solution for simulation of metal AM which enables to build AM parts in timely manner. It is aimed at helping engineers and manufacturers in optimizing their 3D printing processes which saves the manufacturing time and minimizes the material waste by simulating in extreme detail. This software additionally provides a simple programme that allows engineers to simply configure and execute simulations, visualize the printing process and analyse the outcomes. It can also assist users in identifying potential problems such as distortion, cracking and residual stresses in printed specimens. The parametric analysis of this research used TMM due to the necessity of thermal process parameters which can be only modified using this approach. The rectangular specimen has the dimensions of 51.45 mm (length) by 10 mm (height) by 10 mm (width). The conducted simulation included the main SLM method elements such as the substrate plate, the component and support structure as shown in Figure 2(a). As for the support structure method, it was classified as "Materialise" that generates block supports with the shell thickness of 0.3mm and it was defined corresponding to the component. The critical surface angle determines the angle of surfaces from which support structures are

built. It is measured in relation to the z direction which ranges from 0 to 90º. The addition of supports is intended to address fabricating issues for intricate parts with overhanging surfaces that always have low inclined angles. There is a crucial angle that must be maintained during the fabrication of overhanging surfaces; otherwise, the overhanging surface will warp more easily or the entire process to stop due to major warping. When inclined angle $\theta = 60°$, all the overhanging surfaces will be successfully fabricated. The support structure will then be eliminated during the support removal stage.

(a)

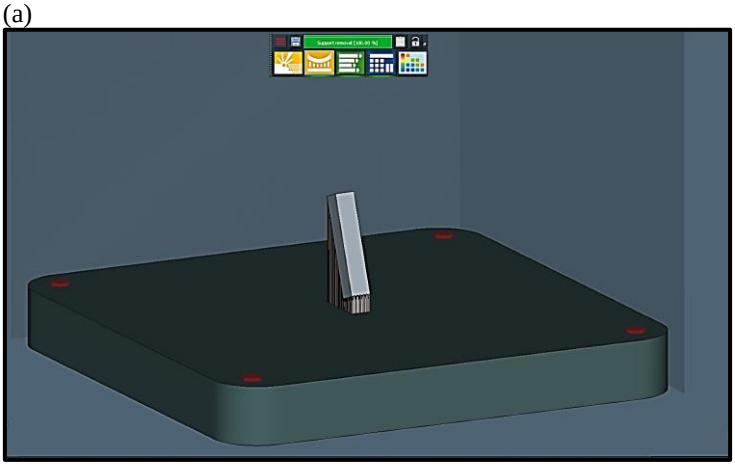

(b)

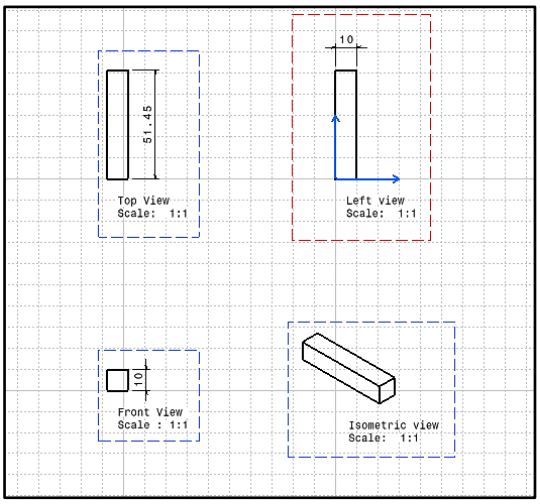

Figure 2. (a) A simulation of rectangular SS316L specimen in 60° of inclination angle from substrate plate on Simufact Additive 2022 and (b) A CAT drawing of the specimen

3.2 Material modelling

In this research, austenitic steel SS316L was selected as the material of specimen. It is commonly used for SLM process due to its outstanding high temperature strength and corrosion resistance which make it appropriate for a variety of applications in the chemical, petrochemical and medical sectors. Other benefits of the chosen material include a specified and international laser powder bed fusion processing standard, as well as commercial powder availability from numerous machine and powder manufacturers [15]. This material has superior heat resistance and may retain the strength and hardness at elevated temperatures.

The basic physical, thermal and mechanical parameters of SS316L powder and base plate used in this research were extracted from the Simufact Additive 2022 software material database as provided in Table 2 and Table 3 and the details are in Figure 3 and Figure 4. In addition to the parameters of the material, the melting temperature was taken to be 1399°C while the solidus temperature was considered as 1371°C. The chemical composition of SS316L powder used to create specimen was described by the powder manufacturer in Table 4.

Table 2: SS316L powder material properties derived from Simufact Additive 2022 Software

Material Properties	SS316L
Density (kg/m³)	7.97e-006
Poisson Ratio (-)	0.30
Yield Strength (MPa)	547
Tensile Strength (MPa)	676
Latent heat for melting	2.65 x 10^5
Latent heat for evaporation	6.09 x 10^6

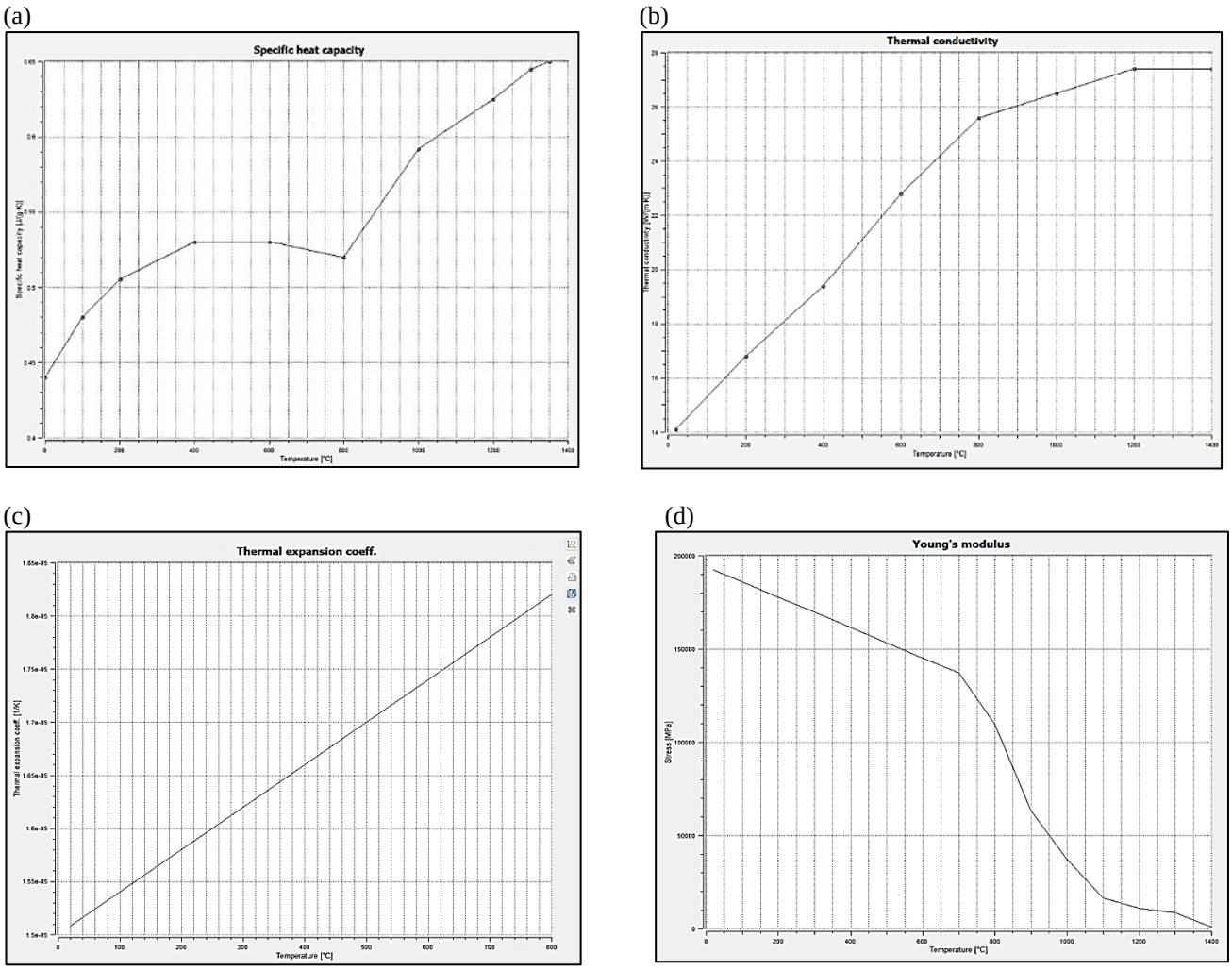

Figure 3. Thermal and Mechanical Properties of SS316L powder based on (a) Specific Heat Capacity (b) Thermal Conductivity (c) Thermal Expansion Coefficient and (d) Young's Modulus

Table 3: SS316L base plate material properties derived from Simufact Additive 2022 Software

Material Properties	SS316L
Density (kg/m³)	7.97e-006
Dissipation factor	0.9
Poisson Ratio (-)	0.30
Latent heat for melting (J/kg)	260000

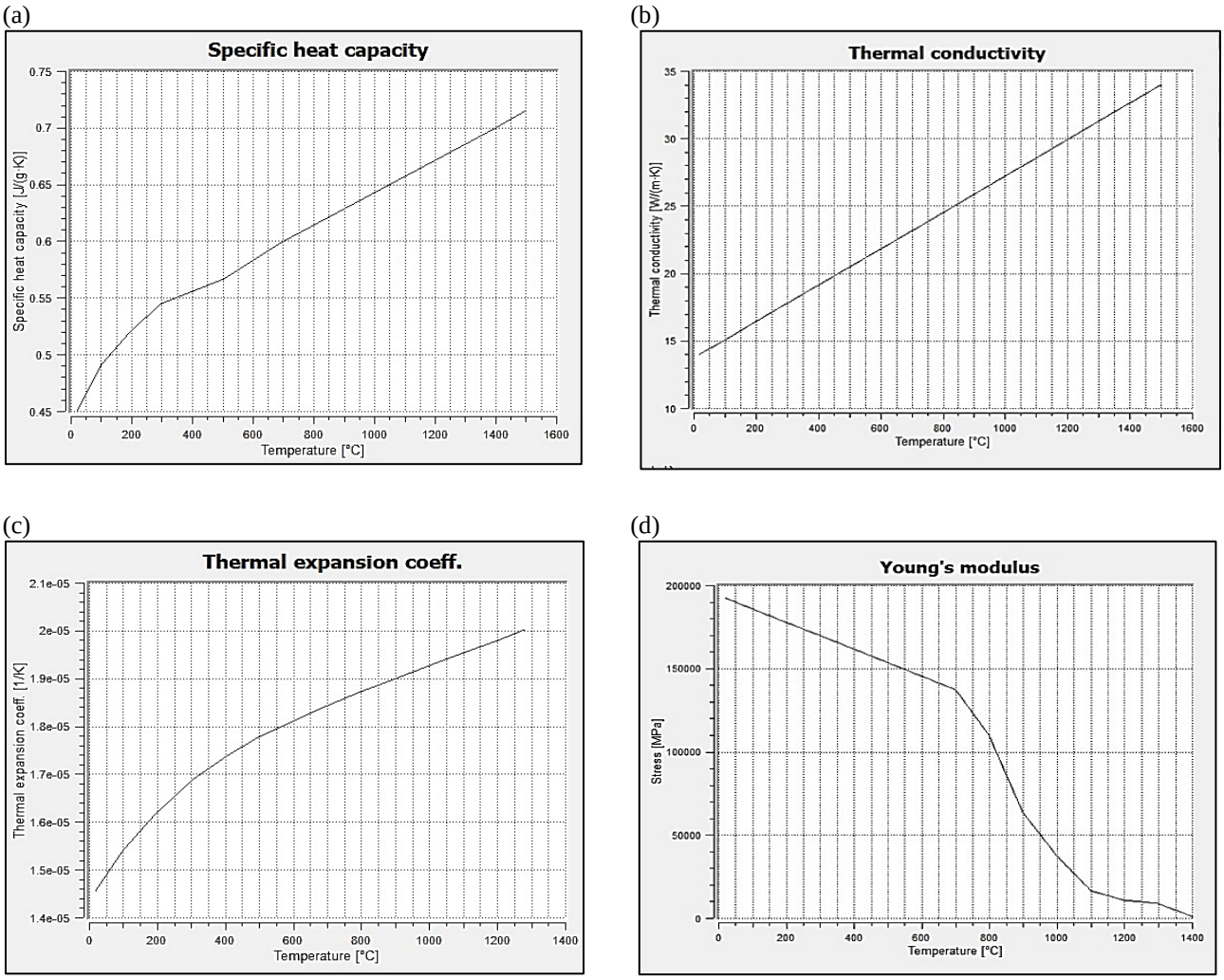

Figure 4. Thermal and Mechanical Properties of SS316L base plate based on (a) Specific Heat Capacity (b) Thermal Conductivity, (c) Thermal Expansion Coefficient and (d) Young's Modulus

Table 4: Chemical composition of the AM powder and base plate in weight % derived from Simufact Additive 2022

Material	C	Cr	Cu	Mn	Mo	N	Ni	P	S	Si
SS316L	0.009	16.82	0.31	1.74	2.08	0.029	10.26	0.03	0.024	0.27

3.3 Process modelling

In accordance with the actual application of the SLM parameters, the simulation defines the layer and laser parameters specified by the manufacturer according to the industry expertise with the chosen material. Thermal and mechanical properties such as thermal conductivity, expansion coefficient, Young's Modulus, and specific heat capacity were considered from the Simufact Additive material data for the numerical computation. The actual SLM parameters from the experimental setup were implemented into the simulation as shown in Table 5.

Table 5: Simulation parameters using Renishaw RenAM 500M for SS316L

Process Parameters	Dimension
Laser beam width (mm)	0.1
Laser power (W)	195
Laser efficiency (%)	25
Laser scanning speed (mm/s)	750
Layer thickness (mm)	0.05
Cooling time (s)	8
Scan rate	4.125×10^{-9}
Hatch distance (mm)	0.11
Layer thickness (mm)	0.05

4.0 EXPERIMENT AND SIMULATION RESULTS

4.1 Experimental of Residual Stress using X-RayBot

Xray-Diffraction is one of the most widely used non-destructive techniques for determining surface residual stress. By combining XRD analysis with electropolishing and consecutive incremental material removal to determine how residual stress evolves with depth, the scope of this technology can be expanded. Residual stress measurements were performed at various measuring points of the specimen. Data were collected using XRD analysis at 10 measuring points on the specimen's left side and 5 measuring points on its right side. XRD measurements were performed using a X-RayBot from MRX-RAYS prepared at Montanuniversität Leoben, Austria. A collimator with a diameter of 2mm was utilized in a psi-mounting configuration with Cr-Kα radiation. The 2θ−sin2(ψ) technique was the basis for the evaluation of analysis. The measurement procedure followed ASTM E915-96 guidelines [16]. The X-ray tube was titled from -40° to +40° while the exposure period for each increment was set to 3s for 25 ψ-increments. The equipment and prepared specimen is shown in Figure 5.

Concentrated acid media like phosphoric acid, sulphuric acid, perchloric acid, acetic acid and their mixed solutions were used for electrochemical polishing. Methanol is often utilized as a solvent in substitute for water. Hence, electropolishing is a method to smooth down the outermost layer of AM specimen. The method involves dipping a cathodic electrode into the solutions and applying direct power to commence a reaction between the specimen's surface and the solutions in order to effectively remove the rough surface [17]. The XRD analysis and electropolishing machines are depicted in the figures below.

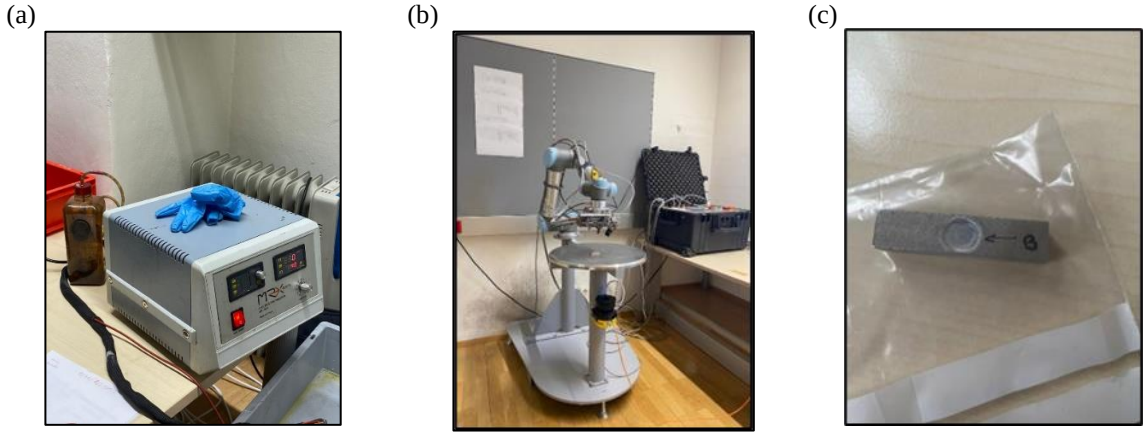

Figure 5. (a) Electrolytic Polisher by MRX-RAY, (b) XRayBot from MRX-RAYS (c) A rectangular specimen which has undergone the electropolishing method

The outcome of electropolishing was a surface with no defined microscopically characteristics such as pits or thorns which made the surface smooth. The directional residual stress was determined on the specimen using the XRD method which calculated the stress tensor based on lattice strain measurements. The XRD measurements are shown in Table 6 and Table 7. The data in the first column in both Tables were obtained by scanning through different depths beneath the specimen's surface, indicating that the data were not influenced by any stress distribution caused by the electropolishing process.

Table 6: XRD data measurements on right side of specimen

Depth (μm)	Residual Stress (MPa)
0	341
75	403
159	633
246	684
335	648

Table 7: XRD data measurements on left side of specimen

Depth (μm)	Residual Stress (MPa)
0	305
50	444
61	562
80	646
102	699
129	701
157	681
199	673
255	644
291	661

4.2 Simulation of Residual Stress Analysis using Simufact Additive

Figure 6 and Figure 7 show the residual stress result of the numerical simulation on the rectangular cuboid specimen. The clipping plane properties and query dialog option were used to determine the residual stress for various depths of Simufact Additive 2022. The multiple stress points must be considered to calculate the average residual stress. The deposition parameters such as laser power, laser speed, rotary axis, scan path and feed rate could be responsible for the residual stress in the AM component.

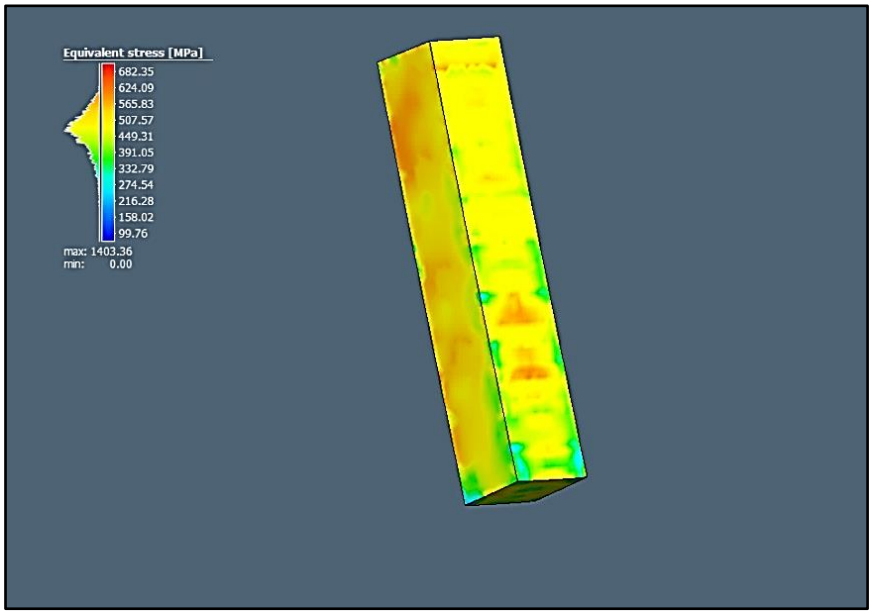

Figure 6. The simulation result of residual stress

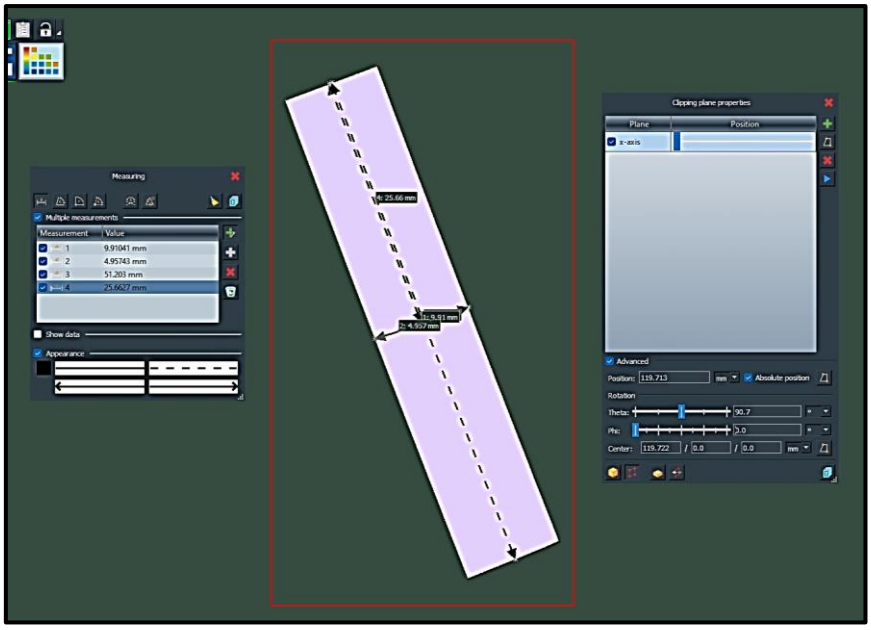

Figure 7. Several residual stress points must be taken to determine the average

Figure 8 illustrates the simulation's adjusted plane angle of specimen that indicates the following deposition of SS316L as the structure deflected to the side at an angle of 0.7°. This deflection was the outcome of the displacement caused by the accumulation of residual stress.

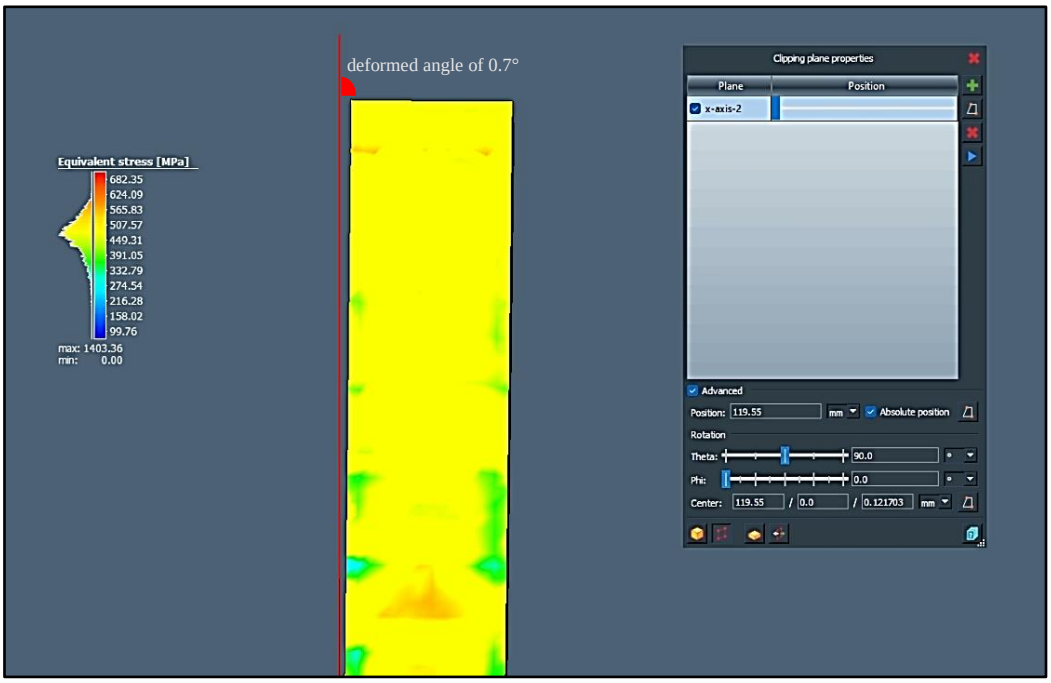

Figure 8. Adjusted plane angle of the specimen SS316L due to deformation

4.3 Result validation

The residual stress tends to be tensile and compressive closer to the core of the part, whereas it is nearer to the surface. Based on a comprehensive investigation, the effects of several parameters such as scanning method, laser power, scanning speed and build orientation on residual stress were analysed. As seen in Figure 9, the results are plotted against depth. The comparison between the experimental diffraction data and the numerical simulation data for the specimen on both sides is shown in this figure. The slope of the left specimen in the simulation was found to be less steep than the experimental data which similarly went to the right side.

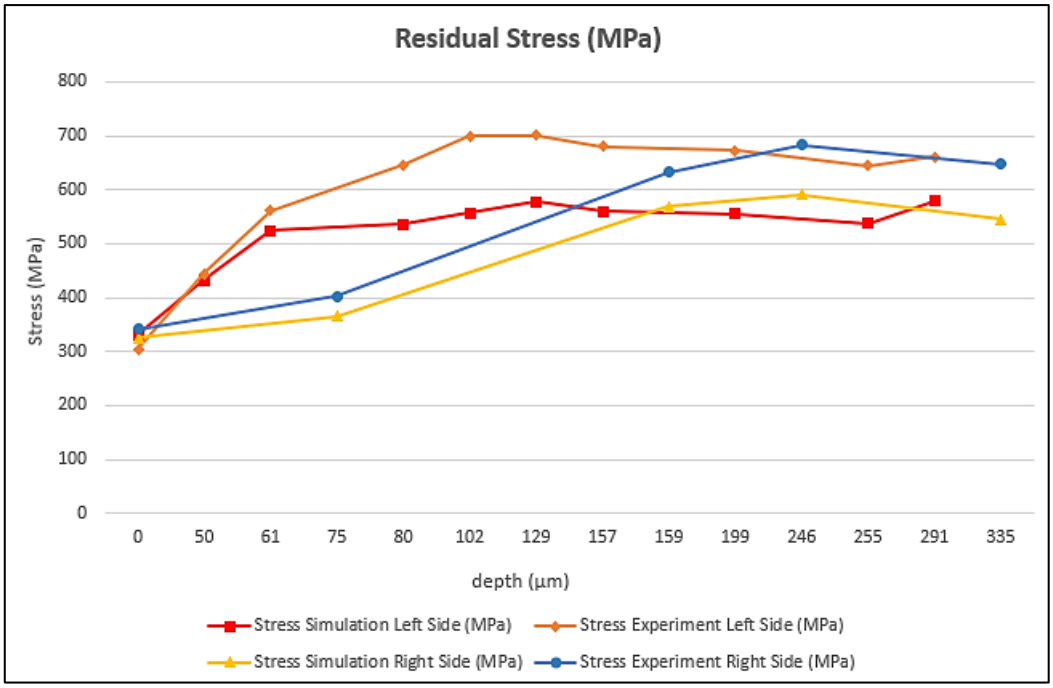

Figure 9. In depth axial residual stress progression of the specimen

The average relative error for the left side was 13.67% which may be obtained by computing the relative error calculation from Equation (1) below. On the other hand, the relative error on the right side was 10.79%. Figure 10 shows the graph of relative error for both sides of the specimen.

$$\text{Relative Error (\%)} = \frac{|\text{Simulation Value} - \text{Experimental Value}|}{\text{Experimental Value}} (100\%) \qquad (1)$$

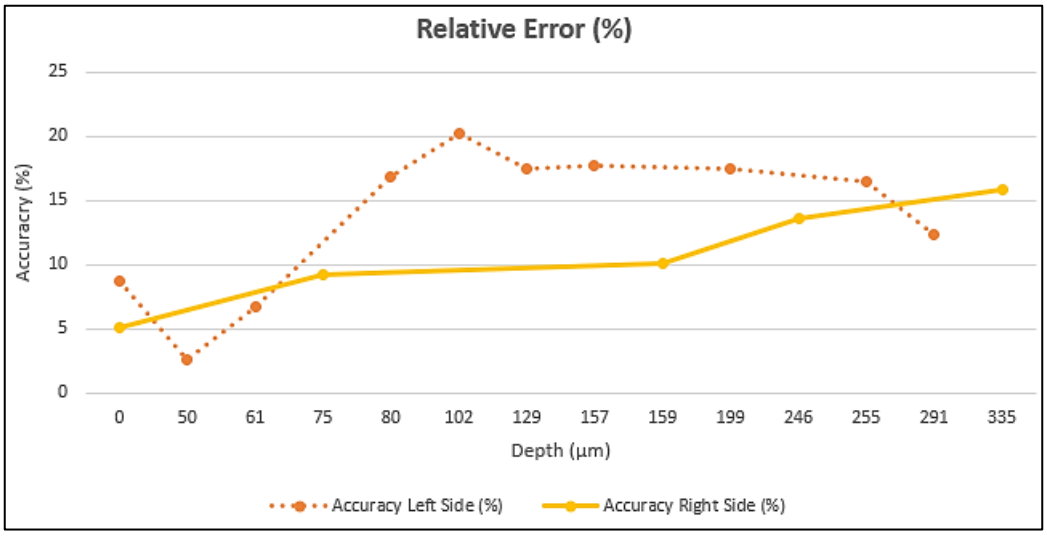

Figure 10. Relative Error graph

5.0 CONCLUSION

This study describes experimental and numerical computation simulations which use the TMM approach in finding the residual stresses. The objective of this study is to compare the results of the experimental data and simulation data of the residual stresses on the left and right surface of SLM specimen. To ensure an accurate comparison between the experimental and simulation case study, the boundary conditions and process parameters are specified in a standardized manner. According to the results of the research, the following conclusions can be drawn:

1. The research on residual stresses of the SLM specimen using Simufact Additive and X-Ray Diffraction method was comprehensive and fulfilled.
2. The test result demonstrates that the chosen process parameters have a significant impact on the originating residual stress.
3. Higher values of residual stresses are seen at the top surface using the X-Ray Diffraction method.
4. For the depth profile of the specimens, the stresses in the surface area initially increase significantly and then fall until one point it begins to rise again.
5. The analysis reveals that the post-treatment can alter residual stresses with a relative inaccuracy of up to 14%.
6. TMM simulation can predict that an SLM specimen will have an acceptable amount of residual stress and it only takes 56 minutes of computer time.
7. After the deposition of SS316L, the adjusted specimen plane angle indicates that the structure deflects to the side by 0.7 degrees. This deflection is made into being as the factor of the deposition of residual tension which results in the displacement shown above.
8. For evaluating complicated geometry, this method is preferred in terms of time management since it is more efficient. In addition, electrolytic polishing is a highly recommended procedure for removing the surface to measure the depth profile of residual stress using X-Ray Diffraction.
9. It is evident from the two comparisons in Figure 9 that simulation could be a reliable resource for designers and engineers to comprehend the development of residual stress during the AM of SS316L.

As a result of the ongoing development of technology, there are quite a few potential methods of research and improvements that may be investigated on the viability of monitoring residual stresses in-process or real-time during the SLM procedure. Research should concentrate on process adjustments for stress control which may be made achievable by developing detectors or methods that provide rapid stress data. Additionally, it is possible to develop and improve numerical simulations that accurately forecast residual stress distributions produced by SLM. Heat transfer and solidification should also be considered for this study.

ACKNOWLEDGEMENT

The author would like to thank the Chair of General Mechanical Engineering in Montanuniversität Leoben, ERASMUS+ KA107 and Smart Manufacturing Research Institute in Universiti Teknologi MARA for their ongoing assistance and guidance during the research.

REFERENCES

[1] Ngo, Tuan D.; Kashani, Alireza; Imbalzano, Gabriele; Nguyen, Kate T.Q.; Hui, David (2018). Additive manufacturing (3D printing): A review of materials, methods, applications and challenges. Composites Part B: Engineering, S1359836817342944–doi: 10.1016/j.compositesb.2018.02.012

[2] Lim, S., Buswell, R. A., Le, T. T., Austin, S. A., Gibb, A. G., & Thorpe, T. (2012). Developments in construction-scale additive manufacturing processes. Automation in construction, 21, 262-268.

[3] Wong, K. V., & Hernandez, A. A review of additive manufacturing. ISRN Mech. Eng. 2012, 1–10 (2012).

[4] Talagani, M. R., DorMohammadi, S., Dutton, R., Godines, C., Baid, H., Abdi, F., ... & Blue, C. (2015). Numerical simulation of big area additive manufacturing (3D printing) of a full-size car. Sampe Journal, 51(4), 27-36.

[5] Salmi, M. (2021). Additive Manufacturing Processes in Medical Applications. Materials, 14(1), 191. doi:10.3390/ma14010191

[6] Yap, C. Y., Chua, C. K., Dong, Z. L., Liu, Z. H., Zhang, D. Q., Loh, L. E., & Sing, S. L. (2015). Review of selective laser melting: Materials and applications. Applied Physics Reviews, 2(4), 041101. doi:10.1063/1.4935926

[7] Laleh, M., Sadeghi, E., Revilla, R. I., Chao, Q., Haghdadi, N., Hughes, A. E., ... & Tan, M. Y. (2022). Heat treatment for metal additive manufacturing. Progress in Materials Science, 101051.

[8] Shiomi, M., Osakada, K., Nakamura, K., Yamashita, T., & Abe, F. (2004). Residual Stress within Metallic Model Made by Selective Laser Melting Process. CIRP Annals, 53(1), 195–198. doi:10.1016/s0007-8506(07)60677-5.

[9] ASTM, F. (2014). 3056: Standard specification for additive manufacturing nickel alloy (UNS N06625) with powder bed fusion. ASTM.

[10] Jawade, S. A., Joshi, R. S., & Desai, S. B. (2021). Comparative study of mechanical properties of additively manufactured aluminum alloy. Materials Today: Proceedings, 46, 9270-9274.

[11] Li, C., Liu, Z. Y., Fang, X. Y., & Guo, Y. B. (2018). Residual stress in metal additive manufacturing. Procedia Cirp, 71, 348-353.

[12] Mercelis, P., & Kruth, J. P. (2006). Residual stresses in selective laser sintering and selective laser melting. Rapid Prototyping Journal.

[13] Mani, Mahesh; Lane, Brandon M.; Donmez, M. Alkan; Feng, Shaw C.; Moylan, Shawn P. (2016). A review on measurement science needs for real-time control of additive manufacturing metal powder bed fusion processes. International Journal of Production Research, 1–19. doi:10.1080/00207543.2016.1223378.

[14] Klute, A., Whittig, L. D., & Allardice, W. R. (1986). X-Ray Diffraction Techniques. Methods of Soil Analysis: Part 1 - Physical and Mineralogical Methods. doi:10.2136/sssabookser5.1. 2ed.c1.

[15] van Belle, L., Vansteenkiste, G., & Boyer, J. C. (2013). Investigation of Residual Stresses Induced during the Selective Laser Melting Process. Key Engineering Materials, 554–557, 1828–1834. https://doi.org/10.4028/www.scientific.net/kem.554-557

[16] Standard, A. S. T. M. E915, 2010," Standard Test Method for Verifying the Alignment of X-Ray Diffraction Instrumentation for Residual Stress Measurement," ASTM International, West Conshohocken, PA, 2003, DOI: 10.1520/E0915-10.

[17] ur Rahman, Z., Deen, K. M., Cano, L., & Haider, W. (2017). The effects of parametric changes in electropolishing process on surface properties of 316L stainless steel. Applied Surface Science, 410, 432-444.